Normal internal coordinates, Force fields and vibrational study of Species Derived from Antiviral adamantadine

Silvia Brandan[1]

[1]Universidad Nacional de Tucumán

May 28, 2020

Abstract

Complete vibrational assignments have been performed for free base, cationic and hydrochloride species derived from antiviral adamantadine by combination of hybrid B3LYP with the 6-31G* and 6-311++G** basis sets and the SQMFF methodology. Normal internal coordinates and scaling factors were used to obtain the harmonic force fields and scaled force constants of three species in gas phase and in aqueous solution. Bond lengths and angles of cationic and hydrochloride species show very good concordances with the experimental of amantadinium azide. The cationic species reveals higher solvation energy value, as compared with antiviral agents, however, brincidofovir, the antiviral used to ebola disease presents a higher reactivity against to adamantadine. Positive value of Mulliken charge on N1 of hydrochloride species in solution could justify the ionic character of H29***Cl30 bond, as evidenced by bond order and AIM calculations. The hydrochloride species is the most reactive in both media while the cationic species the less reactive. High electrophilicity and nucleophilicity indexes of cationic species in both media justify its higher hydration. Good concordances were observed between experimental and predicted 1H and 13C NMR and electronic spectra. In solution, the three species are present as revealed by the experimental UV spectrum of hydrochloride amantadine

1. Introduction

Amantadine, also known as adamantadine has been studied for a long time together with its derivatives because it antiviral agent is indicated to treat influenza A virus infections and, is also used in medicinal chemistry in the treatment of Parkinson's disease [1-28]. Derivatives containing the adamantane group are the great interest in the design of new pharmacological drugs due to that these species present different properties, as suggested by Lamoureux and Artavia [13]. The IUPAC name of adamantamine is adamantan-1-amine hydrochloride and its structure is rigid with three fused cyclohexane rings in chairs conformations [6]. The study of amantadine hydrochloride by using mass spectrum has revealed that the amino substituent is as ionic species, as in the crystalline structure of amantadinium azide [6,29]. So far, the infrared and Raman spectra of amantadine hydrochloride and of free base and cationic species of amantadine were not assigned. These three structures of antiviral amantadine can be seen in **Scheme 1** . The identifications of these species in different media by using a quick and easy technique as is the vibrational spectroscopy are important taking into account the relevancy and uses of amantadine. On the other hand, the combination of theoretical *ab-initio* calculations with the vibrational spectra and the scaled quantum mechanical force field (SQMFF) methodology are very good tools to perform reliable harmonic force fields and force constants, as was suggested by Pulay et al. [30] and, as was reported for species with different fused rings [31-33]. Hence, with that methodology the complete vibrational assignments of those three species of amantadine are possible carried out by using the corresponding normal internal coordinates, transferable scaling factors and the Molvib program [34,35].

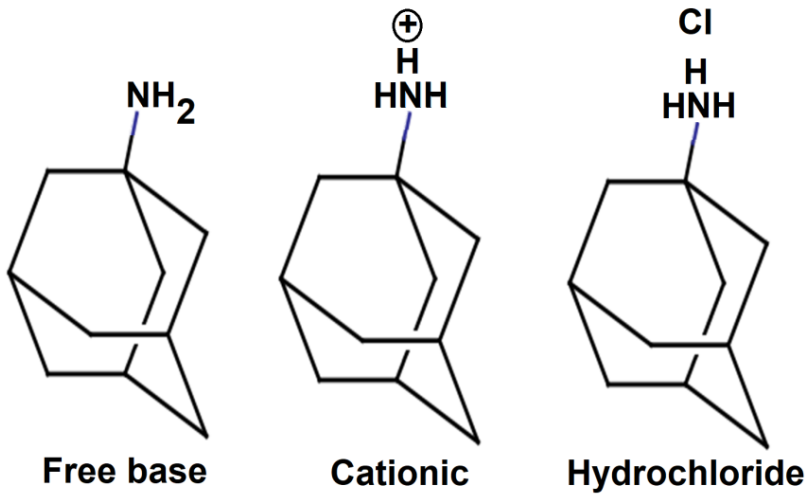

Scheme 1. Structures of free base, cationic and hydrochloride species of amantadine.

Hence, the aims of the work are: (i) to optimize the structures of free base, cationic and hydrochloride species of adamantadine in gas phase and aqueous solution by using functional hybrid B3LYP with the 6-31G* and 6-311++G** basis sets [36,37], (ii) to predict atomic charges, molecular electrostatic potentials, stabilization energies, solvation energies, topological properties and frontier orbitals in both media by using the better basis set and, (iii) to perform the complete vibrational assignments of three species of adamantadine by using the experimental available infrared and Raman spectra, the normal internal coordinates of each species by using the scaled quantum mechanical force field (SQMFF) methodology and the Molvib program [30,34,35]. Then, the predicted properties for the three species of amantadine are compared with other reported for antiviral agents [31,38-40]. In addition, to verify the reproducibility of theoretical optimized structures of free base, cationic and hydrochloride species the predicted ^{1}H- and ^{13}C-NMR spectra were compared with the corresponding experimental ones available from the literature. The ultraviolet-visible spectra for the three species in aqueous solution were also predicted by using the same level of theory.

2. Material and methods

The *GaussView* program [41] was used to model the free base, cationic and hydrochloride structures of amantadine according to that crystalline structure of amantadinium azide [29] while its optimizations in gas phase and aqueous solution were performed with the functional hybrid B3LYP and the 6-31G* and 6-311++G** basis by using the Revision A.02 of Gaussian program [36,37,42]. The IEFPCM and universal solvation methods [43-45] were used to optimized the three structures in solution while with the Moldraw program were calculated the volumes of all species at the same level of theory [46]. To investigate probable intra-molecular interactions, atomic charges, molecular electrostatic potentials, acceptors-donors energies and topological properties were performed with NBO and AIM 2000 programs [47-50]. The differences between both frontier orbitals were also computed to calculate the gap values and the chemical potential (μ), electronegativity (χ), global hardness (η), global softness (S), global electrophilicity index (ω) and global nucleophilicity index (E) descriptors [38-40]. On the other hand, the electronic spectra of three species in aqueous solution were predicted by using the time-dependent DFT calculations (TD-DFT) while the GIAO method was used to predict the ^{1}H and NMR chemical shifts in the same medium [51]. Normal internal coordinates of three species of amantadine and transferable scaling factors were employed in the determination of corresponding harmonic force fields by using the scaled mechanical force field (SQMFF) methodology and the Molvib program [30,34,35]. The normal internal coordinates related to NH_2 group of free base was considered with C_{2v} symmetry while the $NH_3{}^{+}$ groups of cationic and hydrochloride groups with C_{3v} symmetries. In the assignments, only potential energy distribution (PED) contributions [?] 10 %

were used while the Raman predicted in activities were corrected to intensities with recommendable equations [52,53].

3. Results and Discussion

3.1. Optimizations in both media

Optimized theoretical structures of free base, cationic and hydrocloride species of amantadine and atoms labeling can be seen in **Figure 1** . Different positions of rings can be observed in the structures of three amantadine species. Three axial (vertical) and one equatorial (horizontal) fused cyclohexane rings in chairs conformations are identified with different colours in Fig. 1. Thus, the rings R1, R2 and R3 are located in axial position while R4 in equatorial one. The C8-C2-C6-C3-C10-C5 atoms belong to ring of yellow colour R1, the C8-C2-C7-C4-C11-C5 atoms belong to ring of green colour R2, the C7-C2-C6-C3-C9-C4 atoms belong to ring of blue colour R3 and, the C3-C9-C4-C11-C5-C10 atoms correspond to ring of orange colour R4. Here, only the R1, R2 and R3 rings were used in the building of normal internal coordinates and, in order to avoid redundant coordinates due to the fused rings some coordinates corresponding to the rings were removed, as will see later in the section vibrational analysis.

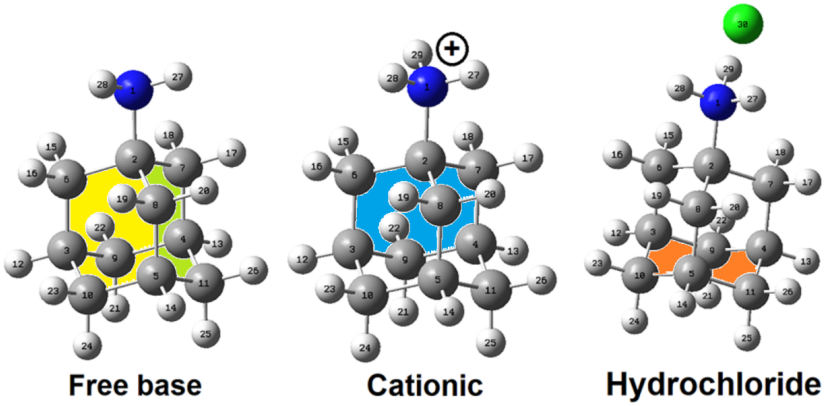

Figure 1. Structures of free base, cationic and hydrochloride species of amantadine and atoms labelling.

The properties calculated by using both hybrid B3LYP/6-311++G** and B3LYP/6-31G* methods are presented in **Table 1** . Thus, total energy uncorrected and corrected by ZPVE for the three amantadine species in both media are presented together with dipolar moment and volume values and their corresponding variations by using both methods. With both basis sets the three species present higher dipole moment values in solution showing the hydrochloride species the higher value while the higher volume is observed for this species by using the B3LYP/6-31G* method.

Table 1. Calculated total energies (E), dipole moments (μ) and volumes (V) of three species of amantadine in gas and aqueous solution phases.

B3LYP/6-311++G** Method	B3LYP/6-311++G** Method	B3LYP/6-311++G** Method	B3LYP/6-311++G** Met
Medium	E (Hartrees)	ZPVE	μ (D)
Free base	Free base	Free base	Free base
GAS	-446.1954	-445.9367	1.27
PCM	-446.2012	-445.9360	2.18
Cationic	Cationic	Cationic	Cationic
GAS	-446.5709	-446.2971	7.86
PCM	-446.6706	-446.2961	11.03

B3LYP/6-311++G** Method	B3LYP/6-311++G** Method	B3LYP/6-311++G** Method	B3LYP/6-311++G** Met
Hydrochloride	Hydrochloride	Hydrochloride	Hydrochloride
GAS	-907.0491	-906.7788	8.70
PCM	-907.0873	-906.7652	14.90
B3LYP/6-31G* Method	B3LYP/6-31G* Method	B3LYP/6-31G* Method	B3LYP/6-31G* Method
Medium	E (Hartrees)	ZPVE	μ (D)
Free base	Free base	Free base	Free base
GAS	-446.0723	-445.8113	1.24
PCM	-446.0771	-445.8165	1.90
Cationic	Cationic	Cationic	Cationic
GAS	-446.4542	-446.1782	8.06
PCM	-446.5527	-446.2770	11.01
Hydrochloride	Hydrochloride	Hydrochloride	Hydrochloride
GAS	-906.8919	-906.6193	8.71
PCM	-906.9278	-906.6526	14.03

Both free base and hydrochloride species in gas phase show practically the same dipole moment values with both methods showing a sligh change in solution. On the other hand, the volumes predicted for the cationic species with both basis sets present almost the same values. Only for free base, the volume variations in both media are influenced by the size of basis set evidencing slight contraction in the volume with the 6-31G* basis set and an expansion volume with the other one. The higher dipole moment values observed for the cationic and hydrochloride species in solution suggest the hydration of both species with water molecules. In addition to the magnitudes, different orientations and directions of dipole moment vectors are observed in the three species in both media with the B3LYP/6-311++G** level of theory. Different positions and directions of these vectors in the three species can be seen in**Figure 2** . Thus, in the free base the vectors are located from centre in direction toward the C5 atom while in the cationic species the vectors are located between the C2-N1 bonds with direction outside. On the contrary, in the hydrochloride species the vectors have its origins closer to C2 atoms and are directed toward the C5-H14 bonds. These different behaviours of vectors can have some influence on the properties of species, especially in aqueous solution. Hence, the solvation energies should be computed in order to see if the dipole moments have effect on those parameters.

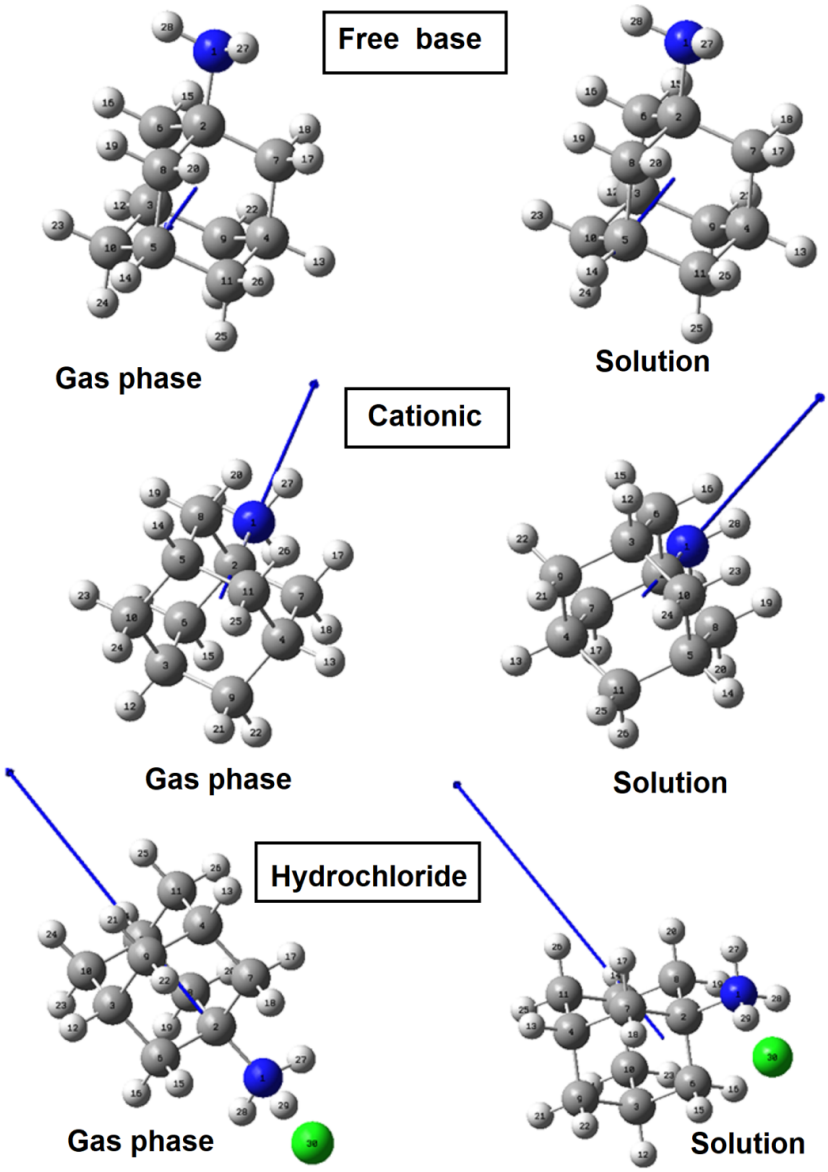

Figure 2. Orientations and directions of dipole moment vectors predicte for the free base, cationic and hydrochloride species of amantadine in both media by using the B3LYP/6-311++G** level of theory.

Therefore, from the differences between the E values in aqueous solution and in gas phase were computed the corrected solvation energies (ΔG_c) taking into account the total non-electrostatic terms. Thus, the ΔG_c values for free base, cationic and hydrochloride species of amantadine by using the hybrid B3LYP/6-311++G** and B3LYP/6-31G* methods are summarized in **Table 2** . These results show that the B3LYP/6-31G* method predict lower solvation energy values for the three species of amantadine and where the cationic species present the higher values because these species are charged in solution. For these reasons, these species with charges are most hydrated in aqueous solution. The free base of amantadine presents two acceptors (N-H) and one donor atom (N) H bonds while the cationic and hydrochloride species have three acceptors and one donor atom H bonds. Hence, in these two latter species are expected higher hydrations, as compared with the free base.

Table 2. Corrected and uncorrected solvation energies by the total non-electrostatic terms of three species of amantadine by using the hybrid B3LYP/6-311++G** and B3LYP/6-31G* methods.

Amantadine[a]	Amantadine[a]	Amantadine[a]	Amantadine[a]
Solvation energy (kJ/mol)	Solvation energy (kJ/mol)	Solvation energy (kJ/mol)	Solvation energy (kJ/mol)
Condition	$\Delta G_{un}{}^{\#}$	ΔG_{ne}	ΔG_{c}
B3LYP/6-311++G** method	B3LYP/6-311++G** method	B3LYP/6-311++G** method	B3LYP/6-311++G** meth
Free base	-15.21	7.86	-23.07
Cationic	-261.51	14.84	-276.35
Hydrochloride	-100.19	14.84	-115.03
B3LYP/6-31G* method	B3LYP/6-31G* method	B3LYP/6-31G* method	B3LYP/6-31G* method
Free base	-12.59	7.73	-20.32
Cationic	-258.36	14.88	-273.24
Hydrochloride	-94.17	14.84	-109.01

$\Delta G_{un}{}^{\#}$: Uncorrected solvation energies; ΔG_{ne}: total non-electrostatic terms; ΔG_{c}: corrected solvation energies.[a]This work.

These values for the three species of amantadine are compared with values predicted with the B3LYP/6-31G* method for antiviral agents such as, isothiazol (-37.51 kJ/mol), thymidine (-116.16 kJ/mol), cidofovir (-169.21 kJ/mol), brincidofovir (-227.34 kJ/mol) and, with the value predicted for foscarnet with the B3LYP/6-311++G** method (-219.64 kJ/mol) [31,38-40]. The differences observed among all values of those species can be justified by the presence of acceptors and donors groups of H bonds. Thus, the free base presents a lower value as compared with isothiazole because this antiviral species has only one N-H bond, two N atoms and the SH and C[?]N groups, hence, a higher hydration is expected for isothiazole ecies in solution. The higher value of cationic species than the other ones obviously is justified by the positive charge because it species shows a higher electrophilicity while the hydrochloride species of amantadine has slightly a lower value than thymidine because this antiviral has other acceptors and donors groups in addition to N-H bond and N atom. On the other side, the antiviral foscarnet agent has a high value because this is a hexa-hydrated trisodic salt and, for this reason, is highly hydrated in solution.

3.2. Geometrical parameters in both media

A very good vibrational analysis request to find the better structure and, for this reason, the theoretical parameters calculated for the three species of amantadine should be compared with the corresponding experimental ones. Thus, in **Table 3** are presented the calculated bond lengths and angles and the dihedral angles for the three species of amantadine in the two media by using the B3LYP/6-311++G** level of theory. Here, the optimized geometrical parameters were compared with the corresponding to amantadinium azide [29] and*N* -(2-Hydroxybenzyl)adamantan-1-aminium chloride [41] by means of the root-mean-square deviation (RMSD) values.

Table 3 . Comparison of calculated geometrical parameters for the free base, cationic and hydrochloride species of amantadine in gas phase and aqueous solution compared with the corresponding experimental ones for amantadinium azide [29] and*N* -(2-Hydroxybenzyl)adamantan-1-aminium chloride.

Parameters	Parameters	B3LYP/6-31G*[a]	B3LYP/6-31G*[a]	B3LYP/6-31G*[a]	B3LYP/6-31G*
		Free base	Free base	Free base	Free base
		Gas	Gas	PCM	PCM
Bond lengths (Å)	Bond lengths (Å)	Bond lengths (Å)	Bond lengths (Å)	Bond lengths (Å)	Bond lengths (
N1-C2	N1-C2	1.469	1.469	1.477	1.477
C2-C6	C2-C6	1.542	1.542	1.540	1.540

Parameters	Parameters	B3LYP/6-31G*[a]	B3LYP/6-31G*[a]	B3LYP/6-31G*[a]	B3LYP/6-31G*
C2-C7	C2-C7	1.542	1.542	1.540	1.540
C2-C8	C2-C8	1.550	1.550	1.546	1.546
RMSD[b]	**RMSD[b]**	**0.031**	**0.031**	**0.026**	**0.026**
RMSD[c]	**RMSD[c]**	**0.026**	**0.026**	**0.021**	**0.021**
Bond angles (º)	Bond angles (º)	Bond angles (º)	Bond angles (º)	Bond angles (º)	Bond angles (º
N1-C2-C6	N1-C2-C6	108.6	108.6	109.1	109.1
N1-C2-C7	N1-C2-C7	108.6	108.6	109.1	109.1
N1-C2-C8	N1-C2-C8	113.6	113.6	112.4	112.4
C6-C2-C7	C6-C2-C7	108.6	108.6	108.8	108.8
C6-C2-C8	C6-C2-C8	108.5	108.5	108.5	108.5
C8-C2-C7	C8-C2-C7	108.5	108.5	108.5	108.5
RMSD[b]	**RMSD[b]**	**2.1**	**2.1**	**1.7**	**1.7**
RMSD[c]	**RMSD[c]**	**2.6**	**2.6**	**2.1**	**2.1**
Dihedral angles (º)	Dihedral angles (º)	Dihedral angles (º)	Dihedral angles (º)	Dihedral angles (º)	Dihedral angles
N1-C2-C8-C5	N1-C2-C8-C5	179.9	179.9	-180.0	-180.0
N1-C2-C6-C3	N1-C2-C6-C3	177.2	177.2	178.2	178.2
N1-C2-C7-C4	N1-C2-C7-C4	-177.2	-177.2	-178.2	-178.2
RMSD[b]	**207.6**	**207.6**	**1.1**	**1.1**	**359.5**
RMSD[c]	**291.0**	**291.0**	**205.7**	**205.7**	**292.3**

[a]This work, [b]Ref [29] for Amantadinium azide; [c]Ref [41] for*N* -(2-Hydroxybenzyl)adamantan-1-aminium chloride. RMSD values in letter bold.

Analyzing in detail table 3, it is possible to observe that the bond lengths and angles for the cationic and hydrochloride species show the lower RMSD values, as expected because those two compared compounds present in its structures NH_3 groups, as those two amantadine species. In general, the structural parameters predicted for the three amantadine species are in agreement with those observed in other experimental structures [54-56]. Besides, for both cationic and hydrochloride species the RMSD values of bond lengths decrease in solution from 0.024-0.018 to 0.012-0.011 Å while the free base species shows RMSD values between 0.031 and 0.021 Å. If now the bond angles are evaluated, it is observed practically a better correlation for cationic and hydrochloride species but the lower RMSD values (2.1-0.2 º) are observed when the predicted values are compared with the experimental parameters of amantadinium azide [29], decreasing in solution, as compared with the values in gas phase. The free base presents RMSD values of bond angles between 2.6 and 1.7 º different from those predicted for cationic and hydrochloride species. A very important result is observed in all dihedral angles because during the optimizations the cationic and hydrochloride species change the signs in significant form but the free base shows the lowest value in solution when they are compared with the corresponding to amantadinium azide [29]. This observation is justified because the free base is protonated in solution, hence, in this species the NH_2group is as NH_3 one. In the hydrochloride species, the dihedral angles show practically highest values because some angles change the signs with the optimization. In general, the dihedral angles present lower RMSD values when these are compared with the corresponding to amantadinium azide [29].

3.3. Charges, molecular electrostatic potential and bond orders studies

Works previous on free base, cationic and hydrochloride S(-) and R(+) species derived of scopolamine alkaloid and antihistaminic promethazine have evidenced that the behaviours of those three species in different media can be quickly explained by atomic charges, molecular electrostatic potentials and bond orders [32,33]. Hence, three types of atomic charges were also analyzed in the three species of amantadine because normally these charges present different values among them and in both media. Hence, atomic Merz-Singh-Kollman (MK), Mulliken and NPA charges together with molecular electrostatic potentials (MEP) and bond orders (BO),

expressed as Wiberg indexes have been calculated for those three species of amantadine in both media by using B3LYP/6-311++G** level of theory. These parameters are presented only for the N1, C2, C6 and C8 atoms in **Table 4** because these atoms structurally form part of C-NH_2 group in the free base and of C-NH_3 groups corresponding to cationic and hydrochloride species (See Fig. 1). In **Figure 3** are given the behaviours of those three charges on the N1, C2, C6 and C8 atoms of three species of amantadine in both media.

Table 4. Mulliken, Merz-Kollman and NPA charges (a.u.), molecular electrostatic potentials (MEP) (a.u.) and bond orders, expressed as Wiberg indexes for the three species of amadantine in gas phase and in aqueous solution by using B3LYP/6-311++G** calculations.

FREE BASE	FREE BASE	FREE BASE	FREE BASE	FREE BASE	FREE
GAS	GAS	GAS	GAS	GAS	GAS
Atoms	MK	Mulliken	NPA	MEP	BO
1 N	-1.067	-0.230	-0.84655	-18.425	2.826
2 C	0.871	-0.279	0.11724	-14.743	3.991
6 C	-0.490	-0.532	-0.38425	-14.788	3.940
8 C	-0.594	-0.516	-0.39244	-14.787	3.945
CATIONIC	CATIONIC	CATIONIC	CATIONIC	CATIONIC	CATI
1 N	-0.823	-0.034	-0.681	-18.101	3.307
2 C	0.673	-0.896	0.159	-14.542	3.919
6 C	-0.486	-0.365	-0.411	-14.619	3.926
8 C	-0.466	-0.365	-0.412	-14.619	3.926
HYDROCHLORIDE	HYDROCHLORIDE	HYDROCHLORIDE	HYDROCHLORIDE	HYDROCHLORIDE	HYDI
1 N	-0.459	-0.089	-0.759	-18.317	3.184
2 C	0.795	-0.499	0.143	-14.695	3.958
6 C	-0.419	-0.432	-0.403	-14.760	3.923
8 C	-0.554	-0.500	-0.396	-14.749	3.939

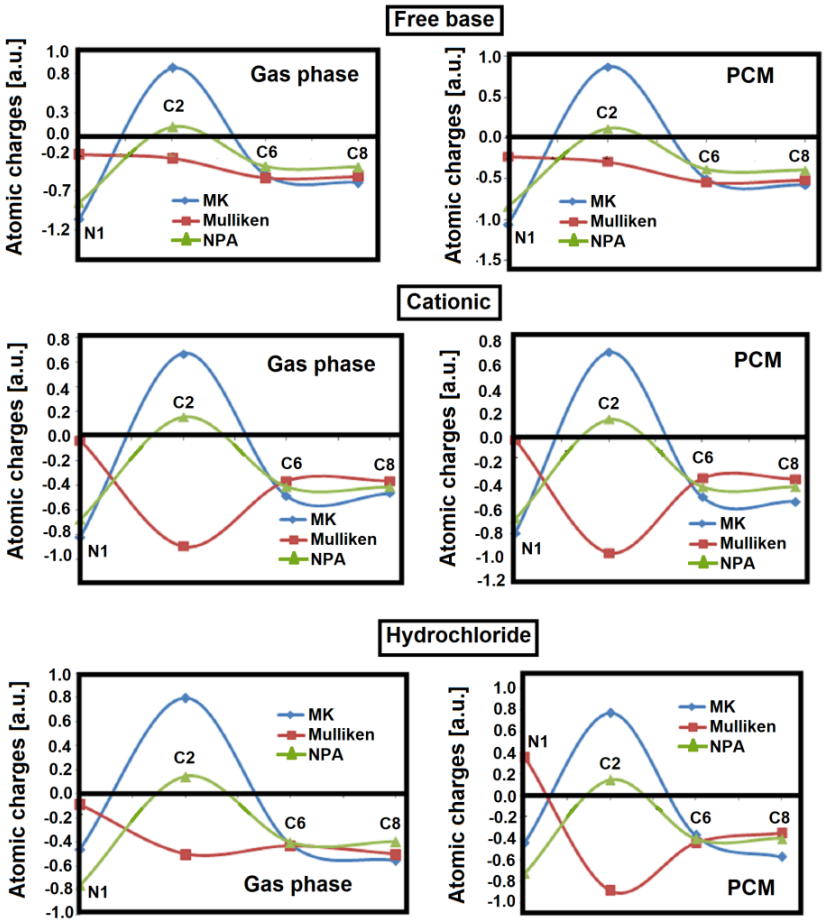

Figure 3. Calculated MK, Mulliken and NPA charges on the N1, C2, C6 and C8 atoms corresponding to the free base, cationic and hydrocloride species of amantadine in both media by using the B3LYP/6-311++G** method.

The exhaustive analyses of figures show that the MK (blue lines) and NPA (green lines) charges present similar behaviours in both media but different from Mulliken charges (red lines). The three charges on C2 atoms of three species in both media present positive values and where the higher values are observed in the MK charges. On the contrary, the Mulliken charges on all C2 atoms show negative values but the higher values are seen on those atoms of cationic and hydrochloride species. Note that the Mulliken charge on the N1 atom of hydrochloride species in solution shows a positive value while the other charges show negative values on these atoms in the two media. This observation could probably be justified by the transformation of covalent H29-Cl30 bond in gas phase between both atoms to ionic N1-H29··· Cl30 bond in solution, as was evidenced by AIM calculations. On the other side, a very important result is that the three charges studies on the C6 atoms of cationic and hydrochloride species show practically the same values and only few differences in the charges corresponding to the free base species in both media are observed.

The molecular electrostatic potentials (MEP) for the three species of amantadine in both media have been calculated by using the Merz-Singh-Kollman scheme by using the same level of theory which can be seen in Table 4. On the atoms of free base, the same values are observed in the two media while slight differences can be seen on the atoms corresponding to the cationic and hydrochloride species. The distributions of charges in the three species are observed quickly in the different colorations shown on the mapped surfaces generate with the *GaussView* program [41]. These red, blue and green colorations on the mapped MEP surfaces of

three species indicate different regions or sites of reactivity, as given in **Figure 4** . Thus, the free base and hydrochloride species show the three colours in different regions different from the cationic one. The free base shows strong red colour on the lone pairs of N1 atom and light blue colours on the H27 and H28 atoms corresponding to NH_2 group while in the hydrochloride species the strong red colour is observed on the C30 atom and the strong blue colours on the three H atoms of NH_3group. On the other hand, the cationic species show blue colours on the entire surface because it is a positively charged species with a high molecular electrostatic potential value (-0.20 a.u.). Then, the red colour indicates nucleophilic sites, the blue colour electrophilic sites while the green regions are inert sites. In these sites are expected that the reactions with potential biological electrophils or nucleophils take place. Hence, different reaction sites are evidenced in the three species of amantadine.

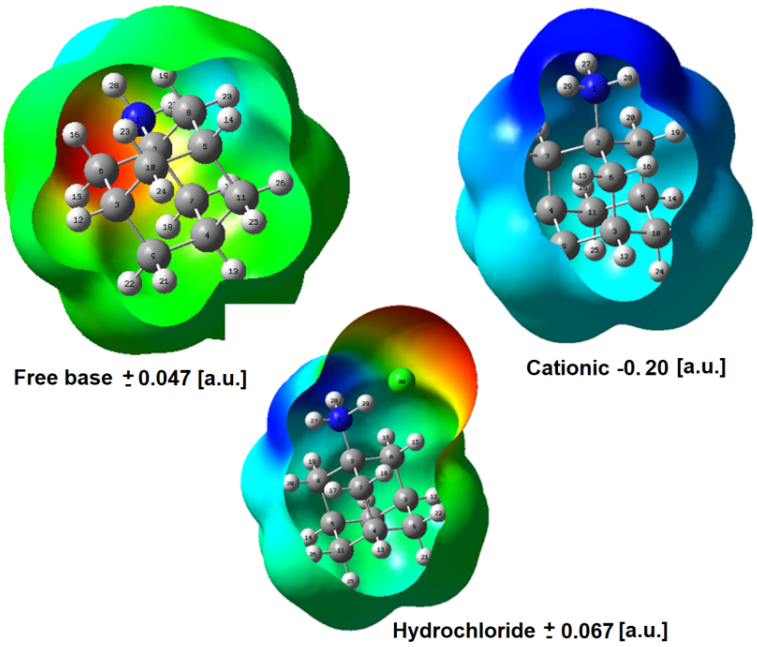

Figure 5. Calculated electrostatic potential surfaces on the molecular surfaces of the free base, cationic and hydrochloride species of amantadine in gas phase. B3LYP functional and 6-311++G** basis set. Isodensity value of 0.005.

These mapped surfaces observed on the free base, cationic and hydrochloride species of amantadine are similar to those S(-) and R(+) species of scopolamine alkaloid and antihistaminic promethazine [32,33].

The bond orders (BO) totals by atom, expressed as Wiberg indexes, have been computed for the three species of amantadine with the NBO program by using the 6-311++G** level of theory [48]. These results for the three species are presented in Table 4. The BOs for the free base present approximately the same values in both media while few differences are observed for the cationic and hydrochloride species. However, the Wiberg bond index matrix in the Natural Atomic Orbital (NAO) basis for the H29-Cl30 bond shows for the hydrochloride species a covalent character in gas phase (0.355) which is transformed to ionic in solution (N1-H29··· Cl30) with a value of 0.123.

3.4. NBO and AIM studies

The studies of stabilities in the three species of amantadine are of interest due to the presence of acceptors (N-H bonds) and donors H bonds (N atom) corresponding to NH_2 and NH_3groups of their structures. These acceptor and donors groups have importance in pharmacological drugs, as in this case [57,58]. Hence, the

intra-molecular interactions can be studied by using the second order perturbation theory analyses of Fock matrix in NBO Basis by using the NBO program and by using the AIM 2000 program [48-50]. First, the studies of donor-acceptor interactions of three species of amantadine in both media by using the NBO program with the B3LYP/6-311++G** method reveal that the free base in both media present the only *LP(1)N1-*C2-C8* interaction with a value of 36.66 kJ/mol in gas phase which decreases to 32.90 kJ/mol in solution. The cationic species does not show interactions in both media while in the hydrochloride species in gas phase are observed the two*LP(1)Cl30-*N1-H29* and *LP(4)Cl30-*N1-H29* interactions with values respectively of 43.22 and 559.16 kJ/mol. In solution, the latter *LP(4)Cl30-*N1-H29* interaction decreases to 125.65 kJ/mol. The higher energy value observed for the hydrochloride species in gas phase (602.38 kJ/mol) indicate that this species is the most stable in both media than the other ones but its stability decreases in solution. On the contrary, the cationic species probably no present interactions due to that this species is hydrated, as supported by high solubility in water of hydrochloride species and to its higher solvation energy.

The Bader's theory of atoms in molecules is practical to investigate the characteristic or nature of different types of interactions such as, intra-molecular, H bonds, ionic, covalent polar, etc., with the topological properties by using the AIM 2000 program [49,50]. Then, in the bond critical points (BCPs) and ring critical points (RCPs) for the three species in both media have been calculated the electron density, $\rho(\rho)$, the Laplacian values, $[?]^2\rho(\rho)$, the eigenvalues $(\lambda 1, \lambda 2, \lambda 3)$ of the Hessian matrix and, the $|\lambda 1|/\lambda 3$ ratio with the B3LYP/6-311++G** method. The results have evidenced that only for the hydrochloride species new H bonds are formed in both media (BCPs) while for the three species are observed the cage critical points (CCPs). These points are formed when several rings form a cage and, for these reasons, the topological properties for ring critical points are not presented here. In **Table 5** are presented the topological properties predicted for CCPs and BCPs of free base, cationic and hydrochloride species by using the B3LYP/6-311++G** method.

Table 5. Analysis of the Bond Critical Points (BCPs) and Ring critical point (RCPs) for the free base and cationic species of amadantine in gas phase and aqueous solution by using the B3LYP/6-31G* method.

B3LYP/6-311++G** Method	B3LYP/6-311++G** Method	B3LYP/6-311++G** Method	B3LYP/6-311++G** Met
Parameter#	Cage critical point	Cage critical point	Cage critical point
	Free base	Free base	Cationic
	Gas	PCM	Gas
ρ(r)	0.0118	0.0119	0.0123
^{2}ρ(r)	0.0724	0.0728	0.0741
λ1	0.0236	0.0237	0.0245
λ2	0.0242	0.0244	0.0246
λ3	0.0244	0.0246	0.0248
|λ1|/λ3	0.9672	0.9634	0.9879
Distances			

#Parameters in a.u., Distances in Å

The ionic or highly polar covalent interactions (BCPs) have$\lambda 1/\lambda 3 < 1$ and $[?]^2\rho(\rho) > 0$ (closed-shell interaction) while the eigenvalues of the Hessian matrix in the CCPs have all positive signs in the three species and approximately the same values in the two media. Molecular graphics of three species in gas can be observed in **Figure 6**showing the H bond interaction (BCPs) of hydrochloride species in red colour while the CCPs if three species in green colours. The only BCPs predicted for the hydrochloride species suggest a high stability for this species in both media. Note that the higher distance observed for that species in solution suggest that the covalent bond in solution is transformed to ionic, as supported by BO study. Besides, if hydrochloride species is ionic, as expected because it is a salt, in solution it is as cationic one, as was also observed in the three S(-) and R(+) species of scopolamine alkaloid and antihistaminic promethazine agent [32,33].

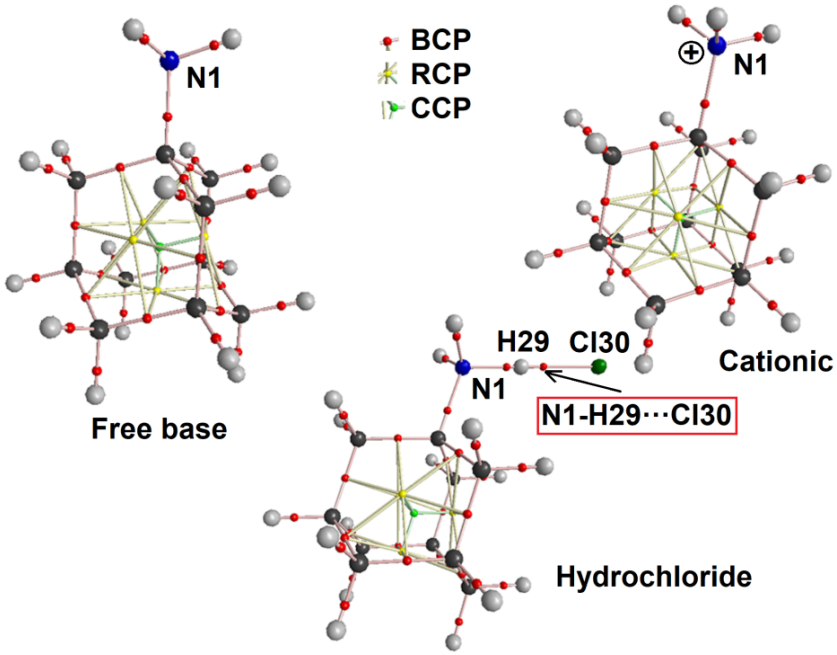

Figure 6. Molecular graphics of three species of amadantine in gas phase showing their H bonds interactions by using the B3LYP/6-311++G** method.

3.5. Frontier orbitals and global descriptors studies

The gap values calculated from the frontier orbitals, HOMO and LUMO are parameters necessary to predict reactivities, as recommended by Paar and Pearson [59] while the behaviours in the different media can be predicted using classical descriptors [31-33,38-40]. In this study, the HOMO, LUMO, energy band gaps and the chemical potential (μ), electronegativity (χ), global hardness (η), global softness (S), global electrophilicity index (ω) and global nucleophilicity index (E) descriptors [32-40] for the three species of amantadine in both media by using the B3LYP/6-311++G** method are summarized in **Table 6** together with the equations used to calculate the descriptors. In **Table 7** are presented these parameters reported for other antiviral agents [31,38-40].

Table 6. Frontier molecular orbitals, HOMO and LUMO, gap values and descriptors for the three amadantine species in gas phase and aqueous solution by using the B3LYP/6-311++G** level of theory.

B3LYP/6-311++G** Method[a]	B3LYP/6-311++G** Method[a]	B3LYP/6-311++G** Method[a]	B3LYP/6-311++G** M
Orbital	FREE BASE	FREE BASE	CATIONIC
	Gas	PCM	Gas
HOMO	-6.4736	-6.5552	-11.6029
LUMO	-0.4218	-0.4299	-4.9253
?GAP?	6.0518	6.1253	6.6776
DESCRIPTORS	DESCRIPTORS	DESCRIPTORS	DESCRIPTORS
χ	-3.0259	-3.0627	-3.3388
μ	-3.4477	-3.4926	-8.2641
η	3.0259	3.0627	3.3388
S	0.1652	0.1633	0.1498
ω	1.9641	1.9914	10.2275
E	-10.4324	-10.6965	-27.5922

[a]This work

χ = - [E(LUMO)- E(HOMO)]/2 ; μ = [E(LUMO) + E(HOMO)]/2; η = [E(LUMO) - E(HOMO)]/2;

$S = \frac{1}{2}\eta$· $\omega = \mu^2/2\eta$· E=μ*i

Table 7. Frontier molecular HOMO and LUMO orbitals, gap and chemical potential (μ), electronegativity (χ), global hardness (η), global softness (S), global electrophilicity index (ω) and global nucleophilicity index (E) for antiviral agents calculated at different levels of theory by using the functional hybrid B3LYP.

B3LYP Method	B3LYP Method	B3LYP Method	B3LYP Method	B3LYP Method	B3LYP Method
Frontier orbitals (eV)	6-31G*	6-31G*	6-31G*	6-31G*	6-311++G**
	Isothiazol[b]	Thymidine[b]	Cidofovir[c]	Brincidofovir[d]	Foscarnet[e]
HOMO	-6.692	-6.1061	-5.9366	-5.5435	-6.9135
LUMO	-2.185	-0.6313	-0.6401	-1.772	-0.6413
|GAP|	4.507	5.4748	5.2965	3.7715	6.2722
DESCRIPTORS	DESCRIPTORS	DESCRIPTORS	DESCRIPTORS	DESCRIPTORS	DESCRIPTORS
χ	-2.2535	-2.7374	-2.6483	-1.8858	-3.1361
μ	-4.4385	-3.3687	-3.2884	-3.6578	-3.7774
η	2.2535	2.7374	2.6483	1.8858	3.1361
S	0.2219	0.1827	0.1888	0.2651	0.1594
ω	4.3710	2.0728	2.0416	3.5474	2.2749
E	-10.0022	-9.2215	-8.7084	-6.8976	-11.8463

[a]From Ref [39], [b]From Ref [38], [c]From Ref [31], [d]From Ref [31], [e]From Ref [40.

Analyzing first Table 6, it is observed that the hydrochloride species in both media have the lower gap values (5.3960 and 4.1116 eV), hence, this species is the most reactive in the two media while the higher gap values observed for the cationic species in both media reveal that that species are the less reactive in both media. Probably, the high electrophilicity and nucleophilicity indexes predicted for the cationic species in both media suggest a higher hydration and low reactivities. The transformation of covalent N1-H29 bond in the hydrochloride species in gas phase to ionic N1-H20···Cl30 in solution support the higher reactivity of this species, as suggested by AIM and bond orders studies. When the gap values predicted for the three amantadine species are compared with the calculated for other antiviral in solution, brincidofovir and isothiazole are clearly the most reactive agents. Maybe, the higher solvation energy of brincidofovir (-227.34 kJ/mol) in relation to that predicted with the same basis set for the hydrochloride species of amantadine (-109.01 kJ/mol) support the higher reactivity of brincidofovir.

3.6. Vibrational study

The three amantadine species have been optimized with C_1 symmetries by using hybrid B3LYP/6-31G* calculations. In the analysis of normal internal coordinates, the NH_2 group of free base was considered with C_{2v} symmetry while the NH_3^+ groups of cationic and hydrochloride groups with C_{3v} symmetries. As was indicated in section 3.1, to avoid redundant coordinates only the R1, R2 and R3 rings in axial position were considered in the building of those coordinates and, due to the fused rings some deformation rings modes were removed. This way, in the coordinates of three species, three deformation rings modes (βR_1, βR_2, βR_3) of R1 were removed, of R2 were removed two deformation rings (βR_1, βR_2) while only βR_1 was removed of R3. For free base species are expected 78 vibration modes while for the cationic and hydrochloride ones 81 and 84 vibration modes, respectively. Due to the C_1 symmetry all these modes have activity in the two infrared and Raman spectra. The experimental available IR and Raman spectra for the free base and hydrochloride species were taken from the literature [6,60,61] and these are compared with those predicted for the three species in **Figures 7** and **8** , respectively. Note that the Raman spectra show very good concordances, in particular, when the predicted spectra in activities were corrected to intensities [52,53].

The normal internal coordinates and the Molvib program were employed to calculate the harmonic force fields for the three species with the scaled quantum mechanical force field (SQMFF) methodology [30,35]. Recommended scaling factors were used together with potential energy distribution (PED) contributions [?] 10 % [34]. Observed and calculated wavenumbers for the three species of amantadine can be seen in **Table 8** . Here, it is necessary to clarify that the experimental available infrared spectra for the hydrochloride species are very different in the higher wavenumbers region, as is observed in **Figure 9** , hence, the bands presented in Table 8 were taken of both spectra. Figure 7 show that in the experimental spectrum of free base the three species could be present because the weak and broad band at 3333 cm^{-1} in the IR spectrum of free base and, at 3434 cm^{-1} in the experimental spectrum of hydrochloride species, are clearly assigned to the anti-symmetric and symmetric NH_3 stretching modes. The other NH_3 anti-symmetric mode in the hydrochloride species is predicted in the infrared spectrum with higher intensity at 1184 cm^{-1} by B3LYP/6-311++G** calculations but very weak in the Raman spectrum while with the scaling by SQM calculations that mode is predicted at 1016 cm^{-1}. Hence, the strong IR band at 1081 cm^{-1} is quickly assigned to that vibration mode.

Figure 7. Experimental available Infrared spectra of free base and hydrochloride species of amantadine in solid phase [6,60

Discussions of most important groups by regions are presented below.

3.6.1. Band Assignments

4000-2000 cm^{-1} region . Characteristic bands related to stretching modes of NH_2, NH_3, CH_2 and C-H groups are expected in this region [31-33,38-40,62]. First, it is observed that the broad and intense IR band observed at 2905 cm^{-1} in the experimental spectrum of hydrochloride species in the higher wavenumbers region overlap all bands predicted for this species in this region.

Table 8 . Observed and calculated wavenumbers (cm^{-1}) and assignments for free base, cationic and hydrochloride species of amantadine in gas phase by using B3LYP/6-311++G** calculations.

Experimental IR[c]	Experimental IR[d]	Experimental Ra[d]	Free base[a] SQM[b]	Free base[a] Assignment[a]	Cationic[a] SQM[b]	Cationic[a] Assignment[a]	Hydrochloride[a] SQM[b]	Hydroc Assignm
3333w	3434m	3334vw	3406	$\nu_a NH_2$	3333	$\nu_a NH_3$	3394	$\nu_a NH_3$
		3334vw	3330	$\nu_s NH_2$	3333	$\nu_a NH_3$	3322	$\nu_s NH_3$
3275w	3191sh	3272vw			3247	$\nu_s NH_3$		
	2975sh	2948sh	2931	$\nu_a CH_2$(C7)	2952	$\nu_a CH_2$(C11)	2956	$\nu_a CH_2$(
2936sh		2936sh	2925	$\nu_a CH_2$(C6)	2946	$\nu_a CH_2$(C9)	2951	$\nu_a CH_2$(
			2921	$\nu_a CH_2$(C11)	2946	$\nu_a CH_2$(C10)	2942	$\nu_a CH_2$(
2924sh		2931vs	2915	$\nu_a CH_2$(C9)	2942	νC3-H12 νC4-H13	2932	$\nu_a CH_2$(
			2915	$\nu_a CH_2$(C10)	2940	νC5-H14 νC4-H13	2925	νC5-H1
		2921sh	2910	νC3-H12	2940	νC3-H12	2924	$\nu_a CH_2$(
			2907	$\nu_a CH_2$(C8)	2925	$\nu_a CH_2$(C6) $\nu_a CH_2$(C7)	2915	νC3-H1
			2902	νC4-H13	2925	$\nu_a CH_2$(C8)	2912	νC4-H13
2907vs	2905vs	2909sh	2900	νC5-H14	2919	$\nu_a CH_2$(C6) $\nu_a CH_2$(C7)	2906	$\nu_a CH_2$(
2898sh		2901sh	2882	$\nu_s CH_2$(C9)	2906	$\nu_s CH_2$(C9)	2897	$\nu_s CH_2$(
			2881	$\nu_s CH_2$(C6)	2904	$\nu_s CH_2$(C10)	2895	$\nu_s CH_2$(

Experimental	Experimental	Experimental	Free base[a]	Free base[a]	Cationic[a]	Cationic[a]	Hydrochloride[a]	Hydroc
2886sh			2881	$\nu_s CH_2$(C10)	2904	$\nu_s CH_2$(C11)	2886	$\nu_s CH_2$(
2853s	2840vs	2868w	2880	$\nu_s CH_2$(C11)	2888	$\nu_s CH_2$(C8)	2885	$\nu_s CH_2$(
						$\nu_s CH_2$(C6)		
2840sh	2840vs	2855w	2875	$\nu_s CH_2$(C7)	2882	$\nu_s CH_2$(C8)	2879	$\nu_s CH_2$(
						$\nu_s CH_2$(C7)		
	2820vs	2840sh	2870	$\nu_s CH_2$(C8)	2881	$\nu_s CH_2$(C6)	2874	$\nu_s CH_2$(
1651w	1617w	1656w					1634	$\delta_a NH_3$
								τN1-H2
		1623w			1583	$\delta_a NH_3$		
1592w	1600m	1596w	1586	δNH_2	1582	$\delta_a NH_3$		
1556w	1504s	1555w					1558	$\delta_a NH_3$ρ
1545sh	1493s	1515w					1458	δCH_2(
1454m	1457m	1463s			1457	δCH_2(C8)	1441	δCH_2(
	1450sh	1443sh	1449	δCH_2(C11)	1438	δCH_2(C9)	1437	δCH_2(
				δCH_2(C10)		δCH_2(C10)		δCH_2(
		1424sh	1430	δCH_2(C6)	1430	δCH_2(C9)	1429	δCH_2(
				δCH_2(C11)				δCH_2(
1442w	1434sh	1424sh	1428	δCH_2(C11)	1428	δCH_2(C10)	1425	δN1H29
				δCH_2(C10)				$\delta_s NH_3$
	1434sh	1424sh	1425	δCH_2(C9)	1418	δCH_2(C6)	1422	δCH_2(
								δCH_2(
			1415	δCH_2(C6)	1416	δCH_2(C7)	1419	δCH_2(
				δCH_2(C7)				δN1H29
1382sh		1408w	1412	δCH_2(C8)	1413	$\delta_s NH_3$		
1368sh			1366	ρCH_2(C8)				
				ρ'C5-H14				
1362w	1361s		1364	wagCH_2(C7)				
1354w		1383w	1358	wagCH_2(C8)			1350	wagCH
				wagCH_2(C10)				$\tau_w NH_3$
1354w	1357w	1348sh	1356	wagCH_2(C9)	1344	ρCH_2(C6)	1341	ρCH_2(
1346w	1333w	1331m	1346	wagCH_2(C10)	1342	ρCH_2(C7)	1339	νC2-C7
				ρC5-H14				νC2-C8
			1325	wagCH_2(C11)	1322	wagCH_2(C9)	1326	wagCH
1313m	1322m	1311m	1316	wagCH_2(C6)	1320	wagCH_2(C10)	1315	wagCH
						wagCH_2(C11)		
	1302m	1307m	1310	wagCH_2(C8)	1309	wagCH_2(C8)	1296	τR_1(A1
						wagCH_2(C6)		
1288sh	1295w	1287sh	1306	τR_1(A1)	1284	ρCH_2(C9)	1289	ρCH_2(
1265w	1277w	1280w	1299	τR_1(A2)	1283	ρCH_2(C11)	1285	νC4-C9
				ρC3-H12				
	1225vw	1275sh			1282	ρCH_2(C10)	1278	wagCH
			1268	ρCH_2(C9)	1269	wagCH_2(C9)	1270	wagCH
						wagCH_2(C11)		wagCH
		1262vw	1266	ρCH_2(C10)	1265	wagCH_2(C6)	1266	wagCH
			1264	ρCH_2(C11)	1263	wagCH_2(C7)	1259	τR_1(A1
						wagCH_2(C8)		τR_2(A1
	1209vw		1242	τR_1(A3)	1249	τR_2(A1)	1253	τR_1(A2
				τR_1(A1)		τR_3(A1)		

Experimental	Experimental	Experimental	Free base[a]	Free base[a]	Cationic[a]	Cationic[a]	Hydrochloride[a]	Hydroc
1189w	1193w	1236vw	1194	ρCH_2(C8)	1247	τR_1(A3) τR_2(A3)	1238	τR_1(A3 τR_2(A3
	1160vw	1199sh	1174	τR_1(A3) ρC5-H14	1237	τR_1(A2)	1208	τR_1(A3 τR_1(A1
1148m	1148vw	1185s	1123	$\rho NH_2 \rho$C4-H13 ρC3-H12	1160	ρC4-H13 ρ'C5-H14 ρ'C3-H12	1167	ρNH_3 ρ'C4-H1
	1118m	1175sh	1114	νC2-N1	1158	ρC5-H14	1151	τR_1(A3
1109sh	1105m	1128sh	1108	ρ'C5-H14 ρ'C3-H12 ρ'C4-H13	1124	ρCH_2(C8)	1125	ρCH_2(C ρCH_2(C ρCH_2(C
1097m	1081s	1119m	1096	ρCH_2(C6) ρCH_2(C7) ρCH_2(C10)	1062	τR_2(A1) τR_2(A2)	1114	$\nu_a NH_3$ $\nu_s NH_3$
		1069w	1066	τR_1(A3) τR_2(A3)	1060	ρC3-H12	1067	ρC4-H1
		1058vw			1059	τR_1(A1) ρC4-H13	1062	ρC3-H1
1045w			1051	τR_1(A1) τR_2(A1)	1053	ρ'C4-H13	1054	ρC5-H1
					1037	τR_1(A1) τR_2(A1)	1052	τR_1(A1 τR_1(A2
			1045	τR_1(A1) τR_1(A2)	1035	τR_2(A3) τR_1(A3)	1049	ρ'C5-H1 ρ'C3-H1
1002w	1081s	989m	1004	νC4-C11 νC3-C10	1024	τR_1(A2)	1016	$\nu_a NH_3$
	1004vw	989m	1003	νC5-C8	1010	νC4-C11	1006	νC4-C1
986w	991vw	989m	995	νC3-C6			995	νC2-C7
		937s			978	τR_2(A3)	979	νC2-N1
967w	970w	937s	970	τR_2(A1) τR_1(A1)	977	νC5-C8	960	$\nu_a NH_3$ τR_1(A1
951w	955w	937s	933	τR_3(A2) τR_3(A1)	935	βR_3(A2) τR_2(A1)	945	τR_3(A1 βR_2(A3
933w					922	βR_3(A3) τR_2(A3)		
	924w		924	τR_2(A3) βR_3(A3)	919	νC4-C11	925	νC3-C9 τwCH_2(
900w	909vw	924sh	903	νC4-C11	877	τwCH_2(C8) τwCH_2(C6)	918	$\nu_a NH_3$ νH29-C νC5-C8
	894vw	867vs	896	νC5-C11 νC5-C10	876	τwCH_2(C10) νC4-C7	896	τwCH_2(νC3-C6 νC4-C7
	879vw	867vs	885	νC5-C8 νC4-C7	874	τwCH_2(C9) τwCH_2(C11) τwCH_2(C7) νC3-C6	889	$\nu_a NH_3$

Experimental	Experimental	Experimental	Free base[a]	Free base[a]	Cationic[a]	Cationic[a]	Hydrochloride[a]	Hydroc
		867vs			863	νC2-C7 ρ'NH_3	879	τwCH_2(τwCH_2(
		867vs	809	τwCH_2(C6)	862	νC2-C8 νC2-C6ρNH_3	874	τwCH_2(
828m	825w	856sh	808	τR_3(A1) τwCH_2(C11) τwCH_2(C8) τwCH_2(C9)	829	νC2-N1	854	τwCH_2(νC2-C6
817w	806w		807	τR_3(A2) τwCH_2(C7) τwCH_2(C10)				
801m	782vw	777w	787	νC3-C9	777	τR_2(A3) τR_3(A2)	799	τR_3(A1 $\tau_w NH_3$
779w	771vw	768sh	778	νC3-C10	774	τR_3(A2) τR_3(A1)	779	τR_2(A3 τR_3(A1
			751	wagNH_2				
724w	717w	713w	745	νC4-C9	740	νC3-C10 νC4-C9 νC5-C11 νC5-C10 νC3-C9	744	νC5-C1 νC3-C1 νC5-C1
669vw	669vw	666sh	689	νC2-C7 νC2-C8 νC2-C6	689	βR_3(A2) νC2-C7	711	τR_3(A2
	662vw	652w			631	τR_3(A2) τR_3(A1)	674	τR_3(A1 τR_3(A2
644vw		646sh	626	βR_3(A3) τR_2(A3)	630	τR_2(A3) βR_3(A3)		
609vw	589vw		621	τR_3(A2) τR_3(A1)			622	τR_2(A3 βR_3(A3
556w	554w	557m					582	$\tau_w NH_3$τ
548w		526sh	528	τR_2(A1) τR_2(A2)			529	βR_2(A3
490#	492vw	499w			501	τR_2(A1) τR_2(A2)	457	τR_1(A2
	469w	478w	436	τR_1(A1) τR_1(A2)	442	τR_1(A1)	438	τR_1(A1
	430w	420w	430	τR_1(A1) τR_1(A3)	438	τR_1(A3)	424	τR_1(A3
		405vw	410	τR_1(A1) τR_2(A1)	408	βR_2(A3)	416	βR_3(A2
			406	βR_3(A3)	405	βR_3(A2)		
	396m		403	βR_3(A2) βR_2(A3)	404	βR_3(A3)		
	384sh	340w	382	τR_2(A1) τR_1(A1) ρC2-N1			396	$\tau_w NH_3$ τR_2(A1

Experimental	Experimental	Experimental	Free base[a]	Free base[a]	Cationic[a]	Cationic[a]	Hydrochloride[a]	Hydroc
	369sh		379	τR_1(A3) ρ'C2-N1	363	τR_2(A1)		
		340w			361	τR_2(A1) τR_2(A2)	383	τR_2(A2
		322sh					327	$\tau_w NH_3$
		322sh					321	ρC2-N1
	303sh	288vw	301	τR_2(A3)	305	τR_2(A3)	305	τR_3(A1
	279sh	263w	266	τR_2(A2) τR_2(A1)	247	τR_2(A2) ρC2-N1	266	τR_2(A1
230#			258	τR_2(A1) τR_3(A3)	246	τR_3(A3) ρ'C2-N1		
		200w	223	$\tau_w NH_2$	184	$\tau_w NH_3$	215	τR_3(A3 ρ'C2-N1
		147w					72	$\tau_w NH_3$ δN1H29
		120w					53	$\tau_w NH_3$

Abbreviations: ν, stretching; wag, wagging; τ, torsion; ρ, rocking; τw, twisting; δ, deformation; a, antisymmetric; s, symmetric; a, antisymmetric; s, symmetric; (A_1), Ring 1; (A_2), Ring 2, (A_3), Ring 3.

[a]This work; [b]From scaled quantum mechanics force field B3LYP/6-311++G** method, [c]From Ref [60], [c]From Ref [60],[d]From Ref [61].[#]From Ref [6].

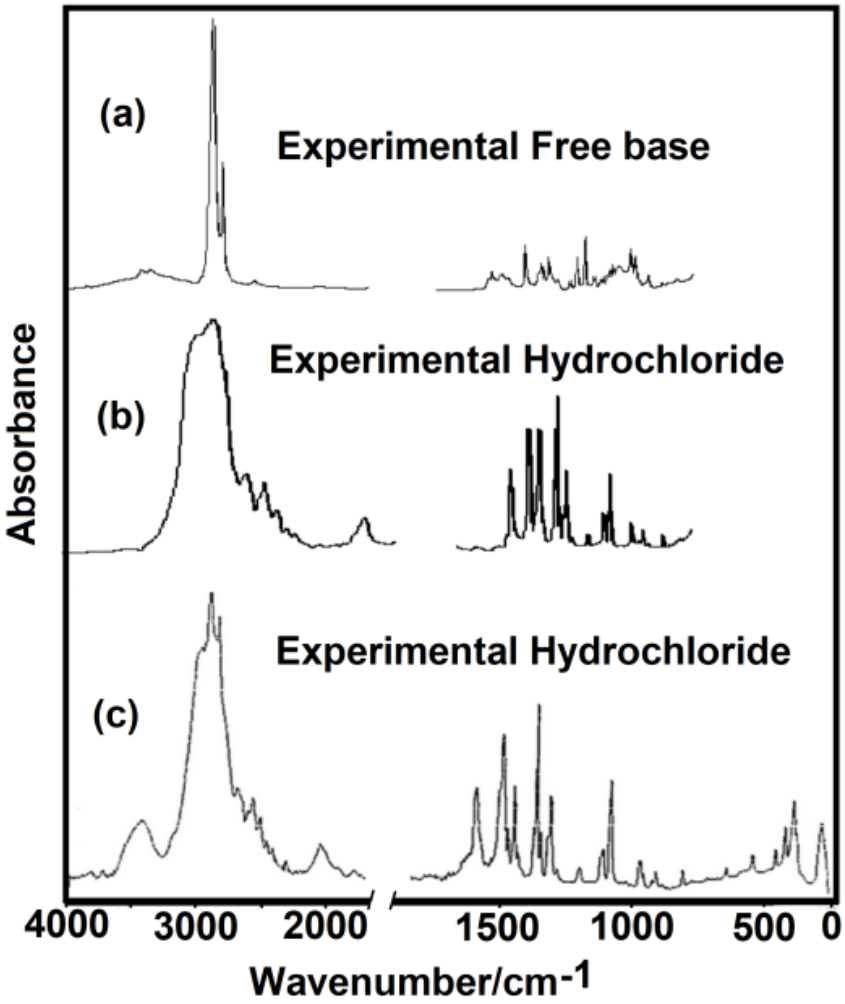

Figure 9. Experimental available Infrared spectra of free base and hydrochloride species of amantadine in solid phase taken from (a) Ref [60], (b) Ref [60] and, (c) Ref [6].

The two NH_2 stretching modes of free base are assigned to the weak IR band at 3333 cm^{-1} while the two NH_3 antisymmetric modes of cationic are assigned to very weak Raman band at 3334 cm^{-1}. In the hydrochloride species one of two NH_3 antisymmetric modes and the symmetric mode are predicted and assigned to the Raman band at 3334 cm^{-1}, as predicted by SQM calculations while the other antisymmetric mode in this species is predicted at 1016 cm^{-1} and assigned to the strong band at 1081 cm^{-1}. The corresponding symmetric mode in the cationic species is predicted at 3247 cm^{-1} and assigned to 3272 cm^{-1}.

1800-1000 cm^{-1} region . In this region, the deformation, wagging and rocking modes of NH_2, NH_3, CH_2 and C-H groups are expected [31-33,38-40,62]. In general, the CH_2 deformations modes are assigned between 1485 cm^{-1} and 1410 cm^{-1} [31-33,38,39,62]. Here, these modes were predicted between 1483 and 1412 cm^{-1}, thus, the bands in this region are assigned to vibration modes of those groups. The weak IR band at 1592 cm^{-1}, observed in Raman at 1596 cm^{-1} is assigned to NH_2 deformation mode of free base. The two anti-symmetric modes of NH_3groups in the cationic species are predicted at 1583 and 1582 cm^{-1} while in the hydrochloride species due to the presence of Cl atom these modes are predicted at 1634 and 1558 cm^{-1}. Therefore, the IR and Raman bands at 1651 and 1556 cm^{-1} are assigned to these modes of hydrochloride

species. The shoulder and weak Raman band at 1424 and 1408 cm^{-1} can be assigned to the corresponding symmetric modes of both species, respectively, because the SQM calculations predict these modes at 1425 and 1413 cm^{-1}. In the three species, the wagging and rocking modes of free base are predicted between 1364/1263 and 1341/1096 cm^{-1}, hence, they can be assigned in these regions, as detailed in Table 8. The NH_3 rocking modes in hydrochloride species are predicted coupled with the deformation mode at 1558 and 1167 cm^{-1} while in the cationic species are predicted at 863 and 862 cm^{-1}, hence, the Raman bands at 1551, 1185 and 867 cm^{-1} are assigned to these vibration modes. On the other hand, the SQM calculations predict the ρH rocking modes in the three species between 1366 and 1049 cm^{-1} and, for this reason, they are assigned in this region.

Skeletal modes. The C2-N1 stretching modes in the three species were predicted in different regions, thus, in the free base, cationic and hydrochloride species this mode is predicted at 1114, 829 and 979 cm^{-1}, respectively. Hence, these modes are associated to the IR and Raman bands observed in these regions. The C-C stretching modes in the three species are assigned as predicted by the SQM calculations in the region between 1004 and 689 cm^{-1}while in the cationic and hydrochloride species at 969 and 988 cm^{-1}, respectively. The C2-C6, C2-C7 and C2-C8 stretching modes in the three species are predicted in different positions, thus, in the free base these modes can be assigned to the weak IR band at 669 cm^{-1} because the calculations predict these modes at 689 cm^{-1}. In the cationic species these modes are predicted at 862 and 689 $cm^{-1}$and, due to Cl atom in the hydrochloride species these modes are shifted toward higher wavenumbers, hence, they are assigned at 1331 and 989 cm^{-1}. Note that the deformations and torsions rings are predicted from 1000 cm^{-1} toward the lower wavenumbers region and in regions expected [31-33,38-40,62]. In general, the calculation predict coupling among them, as observed in Table 8. Other skeletal modes are assigned according to the calculations.

4. Force constants

A set of scaled force constants for the three amantadine species in the two media were obtained from the harmonic force fields calculated by using the B3LYP/6-311++G** level of theory with the SQMFF methodology [30,34] and Molvib program [35]. Consequently, these harmonic force constants are summarized for the three species in both media in**Table 9** . When the values of three species of amantadine are analyzed it is observed that the *φ(νN-H)* force constants of three species are different among them, as expected because these constants for the free base correspond to NH_2 groups while in the cationic and hydrochloride species to NH_3 groups. Thus, in this latter species the values in gas phase are different from those observed in solution where, obviously, the presence of Cl atom justifies these differences. In solution, the BO and AIM studies have evidenced ionic character to H29···Cl30 bond in this media, hence, the force of N1-H29 bonds increases according decreases the force of H29···Cl30 bond. Then, in the hydrochloride species also the C2-N1 bond and the C2-C6, C2-C7 and C2-C8 bonds present differences, as evidenced by vibrational analyses in the shifting of stretching modes related to those bonds. The values of $\varphi(\nu^{\frown}H_2)$ and$\varphi(\delta^{\frown}H_2)$ force constants practically do not show variations in the three species in both media.

Table 9 . Scaled internal force constants for the free base, cationic and hydrochloride adamantine species in gas and aqueous solution phases by using the B3LYP/6-311++G** method.

Force constant	Adamantine[a]	Adamantine[a]	Adamantine[a]	Adamantine[a]	Adamantine[a]	Adamantine[a]
	Free base Gas	Free base PCM	Cationic Gas	Cationic PCM	Hydrochloride Gas	Hydrochloride PCM
$\varphi(\nu N\text{-}H)$	6.31	6.20	6.08	6.07	4.99	5.64
$\varphi(\nu^{\frown}\text{-}N)$	4.38	4.24	2.54	3.14	4.78	3.46
$\varphi(\nu^{\frown}\text{-}H)$	4.63	4.63	4.75	4.72	4.70	4.69
$\varphi(\nu^{\frown}\text{-}^{\frown})_P$	4.50	4.51	4.50	4.55	6.11	4.55
$\varphi(\nu^{\frown}H_2)$	4.64	4.64	4.69	4.69	4.71	4.68
$\varphi(\delta^{\frown}H_2)$	0.71	0.71	0.71	0.71	0.73	0.71

Units are mdyn Å^{-1} for stretching and mdyn Å rad^{-2} for angle deformations

[a]This work.

5. NMR study

The predicted ^{1}H and NMR chemical shifts of three species of amantadine in aqueous solution were predicted by using the GIAO method and the hybrid B3LYP/6-311++G** level of theory. Comparisons between these results with the experimental available^{1}H and NMR chemical shifts of free base and amantadine hydrochloride in $CDCl_3$ are presented in **Tables10** and **11** , respectively by means of the RMSD values [6,60]. The RMSD values show the better correlations for the^{1}H nucleus of free base (0.3 ppm) while the same obtained values for the hydrochloride and cationic species (1.7 ppm) could suggest the presence of both species in solution. On the other hand, the cationic and hydrochloride species present good correlations in the nucleus (4.8-4.5 ppm), as compared with the other one (6.5-4.9 ppm). The differences observed in the RMSD values could be attributed to the different media because the calculations were performed in aqueous solution while the experimental spectra were obtained in $CDCl_3$. These good correlations predicted by the^{1}H and NMR chemical shifts in the three species in solution support the qualities of optimized structures by using the B3LYP/6-311++G** method.

Table 10 . Observed and calculated ^{1}H chemical shifts (δ in ppm) for the three species of amadantine in aqueous solutions by using the B3LYP/6-311++G** method.

H atom	B3LYP/6-311++G**[a]	B3LYP/6-311++G**[a]	B3LYP/6-311++G**[a]	Exp[b]	Exp[c]
	Free base	Cation	Hydrochloride		
12-H	1.87	2.13	2.05	2.05	2.15
13-H	1.87	2.14	2.05	2.05	2.15
14-H	1.84	2.15	2.07	2.05	2.15
15-H	1.51	1.85	2.07	1.76	2.04
16-H	1.42	1.87	1.74	1.76	2.04
17-H	1.42	1.88	1.74	1.76	2.04
18-H	1.51	1.85	2.07	1.76	2.04
19-H	1.52	1.87	1.72	1.76	2.04
20-H	1.52	1.89	1.72	1.76	2.04
21-H	1.68	1.78	1.78	1.42	1.69
22-H	1.61	1.70	1.66	1.42	1.69
23-H	1.58	1.70	1.67	1.42	1.69
24-H	1.63	1.77	1.77	1.42	1.69
25-H	1.63	1.78	1.77	1.42	1.69
26-H	1.58	1.71	1.67	1.42	1.69
27-H	0.65	4.25	3.51	1.28	8.28
28-H	0.65	4.24	3.51	1.28	8.28
29-H		4.25	10.18	1.28	8.28
RMSD[a]	**0.3**	**1.2**	**2.2**		
RMSD[b]	**2.6**	**1.7**	**1.7**		

[a]This work GIAO/B3LYP/6-311++G** Ref. to TMS,[b]From Ref [60], [c]From Ref [6].

Table 11 . Observed and calculated chemical shifts (δ in ppm) for the three species of amadantine in aqueous solutions by using the 6-311++G** method.

C atoms	6-311++G**	6-311++G**	Exp[b]	Exp[c]
Free base	Cation	Hydrochloride		

C atoms		6-311++G**	6-311++G**	Exp[b]	Exp[c]
2-C	51.88	62.64	60.30	47.24	52.95
3-C	35.13	34.72	34.59	29.85	28.97
4-C	35.13	34.82	34.59	29.85	28.97
5-C	35.99	35.01	35.12	29.85	28.97
6-C	46.99	42.88	42.31	46.32	40.56
7-C	46.99	42.70	42.31	46.32	40.56
8-C	53.53	42.76	44.39	46.32	40.56
9-C	40.09	38.23	38.28	36.34	35.38
10-C	39.52	38.09	38.57	36.34	35.38
11-C	39.52	38.10	38.57	46.32	40.56
RMSD[a]	**4.9**	**6.5**	**5.9**		
RMSD[b]	**6.5**	**4.8**	**4.5**		

[a]This work GIAO/B3LYP/6-311++G** Ref. to TMS,[b]From Ref [60], [c]From Ref [6].

6- Electronic spectrum

Hydrochloride amantadine is a species highly soluble in water (250 mg/mL), hence, the experimental available ultraviolet-visible spectrum of that species of amantadine in aqueous solution between 200 and 300 nm was compared in **Figure 10** with the corresponding predicted for free base, cationic and hydrochloride species in the same medium by using the same level of theory [6]. The experimental spectrum show two shoulders at 205 and 222 nm and a weak band in c.a. 270 nm while the UV spectrum of free base predicted a intense band at 140 nm and a weak at 180 nm, in the cationic species the UV spectrum shows a shoulder at 150 nm and a maximum at 170 nm and, finally, in the UV spectrum of the hydrochloride species are predicted a shoulder at 180 nm and a maximum at 265 nm. Here, the UV spectrum of free base cannot be seen experimentally because the experimental spectrum was obtained from 200 to 300 nm. Hence, the free base in solution is as a cationic species, it is confirmed by the band of cationic species in 170 nm while the intense band predicted at 265 nm for the hydrochloride species correspond to that experimental observed at 270 nm. On the other hand, the shoulder observed for the hydrochloride species at 180 nm correspond to cationic species. Hence, the three species are clearly present in the experimental UV spectrum of hydrochloride amantadine in aqueous solution.

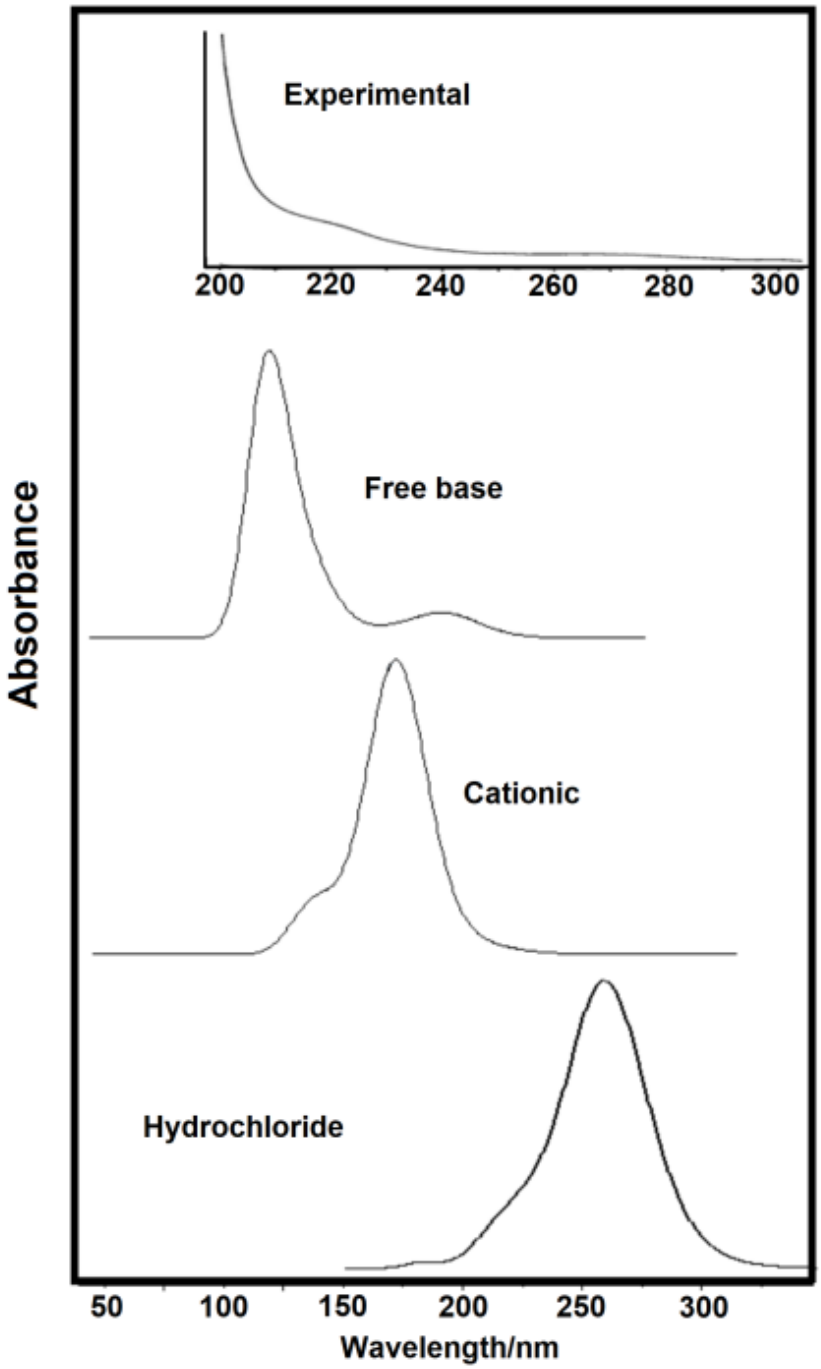

Figure 9 . Experimental available spectrum of hydrochloride amantadine in aqueous solution [6] compared with those predicted for the three species in the same medium by using the B3LYP/6-311++G** method.

8. Conclusions

In this work, the theoretical structures of free base, cationic and hydrochloride species of antiviral adamantadine have been determined by using the functional hybrid B3LYP with the 6-31G* and 6-311++G** basis sets. Complete vibrational assignments of 78, 81 and 84 vibration modes expected for free base, cationic and

hydrochloride species have been performed by combination of functional hybrid B3LYP with the SQMFF methodology. Normal internal coordinates and transferable scaling factors were used to obtain the harmonic force fields and scaled force constants of those three species in gas phase and aqueous solution. The calculations in solution were carried out with the PCM method and the universal solvation model. The bond lengths and angles of cationic and hydrochloride species show very good concordances with those experimental reported for amantadinium azide. The cationic species of adamantadine reveals higher solvation energy value, as compared with other antiviral agents, however, brincidofovir, the antiviral species used to treat of *ebola* disease presents a higher reactivity against to adamantadine species. The positive value of Mulliken charge on the N1 atom of hydrochloride species in solution could justify the ionic character of H29···Cl30 bond, as was evidenced by bond order and AIM calculations. The hydrochloride species is the most reactive in both media while the higher gap values observed for the cationic species in both media reveal that that species are the less reactive in both media. The high electrophilicity and nucleophilicity indexes predicted for the cationic species in both media justify its higher hydration and low reactivity. Good concordances were observed when the experimental ^{1}H and NMR and electronic spectra are compared with the corresponding predicted by calculations. In solution, the three species are present as revealed by the experimental UV spectrum of hydrochloride amantadine in aqueous solution.

Acknowledgements. This work was supported with grants from CIUNT Project Nº 26/D608 (Consejo de Investigaciones, Universidad Nacional de Tucumán). The author would like to thank Prof. Tom Sundius for his permission to use MOLVIB.

References

[1] R.C. Fort, P.R. Schleyer, Adamantane: consequences of the diamondoid structure, Chemical Reviews. 1964, 64, 277-300.

[2] W.L. Davies, R.R. Grunnert, R.F Haff, J.W. McGahen, E.M. Neumeyer, M. Paulshock, J.C. Watts, T.R. Wood, E.C. Hermann, C.E. Hoffmann, Antiviral activity of 1-adamantamine (amantadine), Science, 1964, 144, 862–863.

[3] H.A. Wendel, M.T. Snyder, S. Pell, Trial of amantadine in epidemic influenza, Journal of Clinical Pharmacy and Therapeutics, 1966, 7, 38–43.

[4] Y. Togo, R.B. Hornick, A.T. Dawkins, Studies on induced influenza in man: I. double blind studies designed to assess prophylactic efficacy of amantadine hydrochloride against A2/Rockville/1/65 strain, Journal of the American Medical Association, 1968, 203, 1089–1094.

[5] R.S. Schwab, A.C. England, D.C. Poskanzer, R.R. Young, Amantadine in the treatment of Parkinson's disease, Journal of the American Medical Association, 1969, 208, 1168–1170.

[6] J. Kirschbaum, Amantadine, Analytical Profiles of Drug Substances, Volume 12, 1983, Pages 1-36.

[7] M.A. Abou-Gharbia, W.E. Childers, H. Fletcher, G. McGaughey, U. Patel, M.B. Webb, J. Yardley, T. Andree, C. Boast, R.J. Kucharik, K. Marquis, H. Morris, R. Scerni, J.A. Moyer, Synthesis and SAR of adatanserin: novel adamantyl aryl- and heteroarylpiperazines with dual serotonin 5-HT(1A) and 5-HT(2) activity as potential anxiolytic and antidepressant agents, Journal of Medicinal Chemistry, 1999, 42, 5077-5094,.

[8] E. De Clercq, Antiviral drugs: current state of the art. J Clin Virol. 2001, 22, 73–89.

[9] Y. Sun, P. SYue, X. Chen, W.K. Hong, R. Lotan, The synthetic retinoid CD437 selectively induces apoptosis in human lung cancer cells while sparing normal human lung epithelial cells, Cancer Research, 2002, 62, 2430-2436.

[10] E. De Clercq, Antiviral drugs in current clinical use Journal of Clinical Virology 2004, 30, 115–133.

[11] M.A. Myint, A.G. Blackmanx, E.W. Tan, (±)-Adamantane-1,2-diyl diacetate, Acta Crystallographica, 2005, E61, o3154–o3155.

[12] F. Marsusi, K. Mirabbaszadeh, G.A. Mansoori, Opto-electronic properties of adamantane and hydrogen-terminated sila- and germa-adamantane: A comparative study, Physica E, 2009, 41, 1151-1156.

[13] G. Lamoureux, G. Artavia, Use of the adamantane structure in medicinal chemistry, Current Medicinal Chemistry, 2010, 17(26), 2967-2978.*10.2174/092986710792065027*

[14] J. Liu, D. Obando, V. Liao, T. Lifa, R. Codd, The many faces of the adamantly group in drug design, European Journal of Medicinal Chemistry, 2011, 46, 1949-1963.

[15] E.S. Al-Abdullah, H.H. Asiri, S. Lahsasni, E.E. Habib, T.M. Ibrahim, A.A. El-Emam, Synthesis, antimicrobial, and anti-inflammatory activity, of novel S-substituted and N-substituted 5-(1-adamantyl)-1,2,4-triazole-3-thiols, Drug Design Development and Therapy, 2014, 8, 505-518.

[16] E.S. Al-Abdullah, H.M. Al-Tuwaijri, H.M. Hassan, M.E. Haiba, E.E. Habib, A.A. El-Emam, Antimicrobial and hypoglycemic activities of novel N-Mannich bases derived from 5-(1-Adamantyl)-4-substituted-1,2,4-triazoline-3-thiones, International Journal of Molecular Sciences, 2014, 15, 22995-23010.

[17] S.H.R. Sebastian, M.I. Attia, M.S. Almutairi, A.A. El-Emam, C.Y. Panicker, C.V. Alsenoy, FT-IR, FT-Raman, molecular structure, first order hyperpolarizability, HOMO and LUMO analysis, MEP and NBO analysis of 3-(adamantan-1-yl)-4-(prop-2-en-1-yl)-1H-1,2,4-triazole-5(4H)-thione, a potential bioactive agent, Spectrochimica Acta Part A, Molecular and Biomolecular Spectroscopy, 2014, 132, 295-304.

[18] A.S. Al-Tamimi, A.A. El-Emam, O.A. Al-Deeb, O. Prasad, S.K. Pathak, R. Srivastava, L. Sinha, Structural and spectroscopic characterization of a novel potential anti-inflammatory agent 3-(adamantan-1-yl)-4-ethyl-1H-1,2,4-triazole-5(4H)thione by first principle calculations, Spectrochimica Acta Part A, Molecular and Biomolecular Spectroscopy, 2014, 124, 108–123.

[19] N.G. Haress, F.A.M. Alomary, A.A. El-Emam, Y.S. Mary, C. Y. Panicker, A.A. Al-Saadi, J.A. War, C.V. Alsenoy, Spectroscopic investigation (FT-IR and FT-Raman), vibrational assignments, HOMO-LUMO analysis and molecular docking study of 2-(Adamantan-1-yl)-5-(4-nitrophenyl)-1,3,4-oxadiazole, Spectrochimica Acta Part A, Molecular and Biomolecular Spectroscopy, 2015, 135, 973-983.

[20] M.S. Almutairi, A.M. Alanazi, E.S. Al-Abdullah, A.A. El-Emam, S.K. Pathak, R. Srivastava, O. Prasad, L. Sinha, FT-IR and FT-Raman spectroscopic signatures, vibrational assignments, NBO, NLO analysis and molecular docking study of 2-{[5-(adamantan-1-yl) - 4-methyl - 4H - 1,2,4-triazol-3-yl]sulfanyl}-N,N-dimethylethanamine, Spectrochimica Acta Part A, Molecular and Biomolecular Spectroscopy, 2015, 140, 1–14.

[21] M.B. Shundalau, E.S. Al-Abdullah, E.V. Shabunya-Klyachkovskaya, A.V. Hlinisty, O.A. Al-Deeb, A.A. El-Emam, S.V. Gaponenko, Raman, infrared and DFT studies of N'-(adamantan-2-ylidene) benzohydrazide, a potential antibacterial agent, Journal of Molecular Structure, 2016, 1115, 258-266.

[22] L.H. Al-Wahaibi, H.M. Hassan, A.M. Abo-Kamar, H.A. Ghabbour, A.A. El-Emam, Adamantane-ısothiourea hybrid derivatives:synthesis, characterization, in vitro antimicrobial, and in vivo hypoglycemic activities, Molecules, 2017, 22, 710.

[23] A. Saeed, Z. Ashraf, M.F. Erben, J. Simpson, Vibrational spectra and molecular structure of isomeric 1-(adamantan-1-ylcarbonyl)-3-(dichlorophenyl)thioureas, Journal of Molecular Structure, 2017, 1129, 283–291,. 10.1016/j.molstruc.2016.09.039.

[24] O. Pirali, M. Goubet, V. Boudon, L. D'Accolti, C. Fusco, C. Annese, Characterization of isolated 1-aza-adamantan-4-one (C9H13NO) from microwave, millimeter-wave and infrared spectroscopy supported by electronic structure calculations, Journal of Molecular Spectroscopy, 2017, 338, 6–14,.

[25] M.A.B. Gapol, D.H. Kim, Novel adamantane-based hole transport materials for perovskite solar cells: a computational approach, A European Journal of Physical Chemistry Chemical Physics, 2019, 21, 3857-3867.

[26] H. Nasrallah, J. Hierso, Porous Materials Based on 3-Dimensional Td-Directing Functionalized Adamantane Scaffolds and Applied as Recyclable Catalysts, Chemistry of Materials, 2019, 31, 619-642.

[27] S.B. Elavarasi, D. Mariam, M.U. Momeen, J. Hu, M. Guin, Effect of fluorination on bandgap, first and second order hyperpolarizabilities in lithium substituted adamantane: A time dependent density functional theory, Chemical Physics Letters, 2019, 715, 310-316.

[28] M. Karakaya, Complexation Energies and Electronic-Structural Properties of Adamantane Derivatives: A DFT Study, Adıyaman University Journal of Science, 2019, 9(2), 290-302. 10.37094/adyujsci.546498

[29] Q. Wang, W.-L. Pan, W. Tang, C.-W. Hu, Amantadinium azide, Acta Cryst. (2007). E63, o2688. https://doi.org/10.1107/S1600536807019630

[30] P. Pulay, G. Fogarasi, G. Pongor, J.E. Boggs, A. Vargha, Combination of theoretical ab initio and experimental information to obtain reliable harmonic force constants. Scaled quantum mechanical (QM) force fields for glyoxal, acrolein, butadiene, formaldehyde, and ethylene. J. Am. Chem. Soc., 1983, 105, 7073.*https://doi.org/10.1021/ja00362a005*

[31] D. Romani, S.A. Brandán, Effect of the side chain on the properties from cidofovir to brincidofovir, an experimental antiviral drug against to Ebola virus disease, Arabian Journal of Chemistry 2019, 12, 2959–2972.*http://dx.doi.org/10.1016/j.arabjc.2015.06.030*

[32] R.A. Rudyk, M.A. Checa, C.A.N. Catalán, S.A. Brandán, Structural, FT-IR, FT-Raman and ECD studies on the free base, cationic and hydrobromide species of scopolamine alkaloid, J Mol. Struct. 2019, 1180, 603-617. *https://doi.org/10.1016/j.molstruc.2018.12.040*

[33] M.E. Manzur, S.A. Brandán, S(-) and R(+) Species Derived from Antihistaminic Promethazine Agent: Structural and Vibrational Studies, Heliyon 2019, 5, e02322.

https://doi.org/10.1016/j.heliyon.2019.e02322.

[34] G. Rauhut, P. Pulay, Transferable Scaling Factors for Density Functional Derived Vibrational Force Fields. J. Phys. Chem. 1995, 99, 3093-3100,*https://doi.org/10.1021/j100010a019*

[35] T. Sundius, Scaling of ab-initio force fields by MOLVIB. Vib. Spectrosc. 2002, 29, 89-95,*https://doi.org/10.1016/S0924-2031(01)00189-8.*

[36] A.D. Becke, Density-functional exchange-energy approximation with correct asymptotic behavior, Phys. Rev. 1988, A38, 3098-3100.

[37] C. Lee, W. Yang, R.G. Parr, Development of the Colle-Salvetti correlation-energy formula into a functional of the electron density. Phys. Rev. 1988, B37, 785-789.

[38] M.B. Márquez, S.A. Brandán, A structural and vibrational investigation on the antiviral deoxyribonucleoside thymidine agent in gas and aqueous solution phases, International J. of Quantum Chem. 2014, 114(3), 209-221. *DOI: 10.1002/qua.24545*

[39] D. Romani, M.J. Márquez, M.B. Márquez, S.A. Brandán, Structural, topological and vibrational properties of an isothiazole derivatives series with antiviral activities, J. Mol. Struct. 2015, 1100, 279-289.*http://dx.doi.org/10.1016/j.molstruc.2015.07.038*

[40] M.A. Iramain, S.A. Brandán, Structural and vibrational study on the acid, hexa-hydrated and anhydrous trisodic salts of antiviral drug Foscarnet, Drug Designing & Intellectual Properties International Journal 2018, 1(3), 1-17.

[41] A.B. Nielsen, A.J. Holder, Gauss View 5.0, User's Reference, GAUSSIAN Inc., Pittsburgh, PA, 2008.

[42] M.J. Frisch, G. W. Trucks, H.B. Schlegel, G.E. Scuseria, M.A. Robb, J.R. Cheeseman, G. Scalmani, V. Barone, B. Mennucci, G.A. Petersson, H. Nakatsuji, M. Caricato, X. Li, H.P. Hratchian, A.F. Izmaylov, J. Bloino, G. Zheng, J.L. Sonnenberg, M. Hada, M. Ehara, K. Toyota, R. Fukuda, J. Hasegawa, M. Ishida, T.

Nakajima, Y. Honda, O. Kitao, H. Nakai, T. Vreven, J.A. Montgomery, Jr, J.E. Peralta, F. Ogliaro, M. Bearpark, J.J. Heyd, E. Brothers, K. N. Kudin, V.N. Staroverov, R. Kobayashi, J. Normand, K. Raghavachari, A. Rendell, J.C. Burant, S.S. Iyengar, J. Tomasi, M. Cossi, N. Rega, J.M. Millam, M. Klene, J.E. Knox, J.B. Cross, V. Bakken, C. Adamo, J. Jaramillo, R. Gomperts, R.E. Stratmann, O. Yazyev, A.J. Austin, R. Cammi, C. Pomelli, J.W. Ochterski, R.L. Martin, K. Morokuma, V.G. Zakrzewski, G.A. Voth, P. Salvador, J.J. Dannenberg, S. Dapprich, A.D. Daniels, O. Farkas, J.B. Foresman, J.V. Ortiz, J. Cioslowski, and D.J. Fox, Gaussian, Inc., Wallingford CT, 2009.

[43] S. Miertus, E. Scrocco, J. Tomasi, Electrostatic interaction of a solute with a continuum. Chem. Phys. 1981, 55, 117–129.

[44] J. Tomasi, J. Persico, Molecular Interactions in Solution: An Overview of Methods Based on Continous Distributions of the Solvent, Chem. Rev. 1994, 94, 2027-2094.

[45] A.V. Marenich, C.J. Cramer, D.G. Truhlar, Universal solvation model based on solute electron density and a continuum model of the solvent defined by the bulk dielectric constant and atomic surface tensions, J. Phys. Chem. 2009, B113, 6378-6396.

[46] P. Ugliengo, MOLDRAW Program, University of Torino, Dipartimento Chimica IFM, , 1998.

[47] B.H. Besler, K.M. Merz Jr, P.A. Kollman, Atomic charges derived from semiempirical methods, J. Comp. Chem. 1990, 11, 431-439.

[48] E.D. Glendening, J.K. Badenhoop, A. D. Reed, J. E. Carpenter, F. Weinhold, NBO 3.1; Theoretical Chemistry Institute, University of Wisconsin; Madison, WI, 1996.

[49] R.F.W. Bader, Atoms in Molecules, A Quantum Theory, Oxford University Press, Oxford, 1990, ISBN: 0198558651.

[50] F. Biegler-Köning, J. Schönbohm, D. Bayles. AIM2000; A Program to Analyze and Visualize Atoms in Molecules, J. Comput. Chem. 2001, 22, 545.

[51] R. Ditchfield, Self-consistent perturbation theory of diamagnetism. I. A gage-invariant LCAO (linear combination of atomic orbitals) method for NMR chemical shifts, Mol Phys. 1974, 27, 714–722.

[52] G. Keresztury, S. Holly, G. Besenyei, J. Varga, A.Y. Wang, J.R. Durig. Vibrational spectra of monothiocarbamates-II. IR and Raman spectra, vibrational assignment, conformational analysis and ab initio calculations of S-methyl-N,N-dimethylthiocarbamate Spectrochim. Acta, 1993, 49A, 2007-2026.

[53] D. Michalska, R. Wysokinski, The prediction of Raman spectra of platinum(II) anticancer drugs by density functional theory, Chemical Physics Letters, 2005, 403, 211-217.

[54] T. Rong, N-(2-Hydroxybenzyl)adamantan-1-aminium chloride, Acta Cryst. (2011).*E67*, o1602. https://doi.org/10.1107/S1600536811020794

[55] X.-D. Jin, X.-Y. Yin, L.-S. Xu, C.-H. Ge and X.-H. Chang, 2-[(Adamantan-1-yl)aminomethyl]-4-chlorophenol hemihydrate, Acta Cryst. 2012, E68, o3296. https://doi.org/10.1107/S1600536812045175

[56] S. Mohamed, D. P. Karothu and P. Naumov, Using crystal structure prediction to rationalize the hydration propensities of substituted adamantane hydrochloride salts, Acta Cryst. 2016, B72, 551-561. https://doi.org/10.1107/S2052520616006326

[57] D.F. Veber. S.R. Johnson, H-Y Cheng, R. Brian, K.W. Ward, K.D. Kopple, Molecular Properties that influence the oral bioavailability of drug candidates, J. Med. Chem. 2002, 45, 2615-2623.

[58] C.A. Lipinski, F. Lombardo, B.W. Dominy, P.J. Feeney. Experimental and computational approaches to estimate solubility and permeability in drug discovery and development setting, Advanced Drug Delivery Reviews, 2001, 46, 3-26.

[59] Parr, R.G., Pearson, R.G. Absolute hardness: companion parameter to absolute electronegativity, J. Am. Chem. Soc. 1983, 105, 7512-7516. *https://doi.org/10.1021/ja00364a005.*

[60] Experimental available Infrared spectrum from: https://webbook.nist.gov/cgi/cbook.cgi?ID=C768945&Mask

[61] Experimental available Infrared spectrum and ^{1}H-, ^{13}C-NMR spectra from: http://drugapprovalsint.com/amantadine-hydrochloride/

[62] S. Trabelsi, N. Issaoui, S.A. Brandán, F. Bardak, T. Roisnel, A. Atac, H. Marouani, Synthesis and physic-chemical properties of a novel chromate compound with potential biological applications, bis(2-phenylethylammonium) chromate(VI), J Mol. Struct. 2019, 1185, 168-182.*https://doi.org/10.1016/j.molstruc.2019.02.106*

Hosted file

`Cover Letter.doc` available at https://authorea.com/users/327116/articles/454788-normal-internal-coordinates-force-fields-and-vibrational-study-of-species-derived-from-antiviral-adamantadine